Bifurcation of the edge-state width in a two-dimensional topological insulator

Hyeonjin Doh*
Department of Physics and Center for Computational Studies of Advanced Electronic Material Properties, Yonsei University, Seoul 120-749, Korea

Gun Sang Jeon†
Department of Physics, Ewha Womans University, Seoul 120-750, Korea

(Received 17 June 2013; published 11 December 2013)

We examine the properties of edge states in a two-dimensional topological insulator. Based on the Kane-Mele model, we derive coupled equations for the energy and the effective width of the edge states at a given crystal momentum in a semi-infinite honeycomb lattice with a zigzag boundary. It is revealed that, in a one-dimensional Brillouin zone, the edge states merge into continuous bands of the bulk states through a bifurcation of the edge-state width. We discuss the implications of the results for experiments in monolayer or thin-film topological insulators.

DOI: 10.1103/PhysRevB.88.245115 PACS number(s): 73.20.At, 71.70.Ej, 72.25.Dc

I. INTRODUCTION

Topological insulators (TIs) are a fascinating field of research and have attracted much interest in condensed-matter physics over the past decade.[1,2] This phenomenon can be traced back to the quantum Hall effect (QHE) in two-dimensional (2D) systems in large magnetic fields. The QHE is characterized by the presence of gapless edge states with a finite band gap in the bulk. This metallic edge channel occurs in TIs with time-reversal symmetry (TRS) preserved. The edge states are also known to be topologically protected, as is the case with the QHE.

TIs were first investigated theoretically in 2D systems,[3,4] dubbed the quantum spin Hall effect, where spin-orbit coupling (SOC) is significant.[5–8] This work was subsequently generalized to the TI in three-dimensional (3D) systems with a single Dirac-cone dispersion at the surface.[9–11] The existence of a TI state of 2D systems has been confirmed by experimental transport measurements in HgTe/CdTe quantum wells.[12,13] The existence of 3D topological insulators is also supported by angle-resolved photoemission spectroscopy (ARPES) measurements in Bi_xSb_{1-x},[14] Bi_2Se_3,[15] and Bi_2Te_3.[16,17] This is consistent with the density of states of the metallic surface observed using scanning tunneling microscope (STM) measurements of $Bi_{1-x}Sb_x$[18] and Bi_2Te_3.[19]

Although the ARPES and STM measurements support the existence of surface states in TIs, the transport measurements are less conclusive because of residual carriers in the bulk states. These residual carriers are attributed to imperfections in the bulk crystals, such as antisite or vacancy defects. Numerous efforts to reduce the bulk carrier density have been made, including chemical doping on Bi_2Se_3 with Sb[20] or on Bi_2Te_3 with Sn.[21] However, a sufficient reduction of the bulk carrier density to suppress completely the bulk contribution of the transport has not been achieved because of the difficulty in fine tuning the doping concentration. An alternative method of controlling the bulk carrier density is to reduce the sample size or to apply a gate voltage. Epitaxially grown thin films of Bi_2Se_3 exhibit a weak antilocalization effect with a large magnetic field, which represents the surface states of a TI.[21] Nonetheless, a reduction in the sample size inevitably induces a gap in the metallic dispersion relation of the TI due to the overlap of the surface states at the two opposite surfaces.[22,23] In 2D TIs, attempts have been made to describe the properties of the edge states.[13,24] Interesting effects of interactions on the edges have also been studied both analytically and numerically.[25–28] In spite of the achievements of earlier works, a good general understanding on the edge states is still lacking in many aspects. In particular, systematic investigation of the dependence of the edge states on various physical parameters is required, which is a main focus of the work reported here.

In this paper, we report a theoretical investigation of the spatial variation in the edge states in a 2D TI. Many theoretical models have been proposed to understand TIs; the Kane-Mele (KM) model[3,29] predicts a bulk energy gap of the honeycomb lattice due to the SOC, but the edge states at the boundaries show a linear metallic dispersion relation inside the bulk gap. Although established TIs do not have a honeycomb lattice, the essential physics captured in this model is believed to give useful insights into the TI phenomenon. We focus on the spatial dependence of the edge-state wave functions at a zigzag boundary. We define an edge-state width, which is a convenient measure of how tightly the edge state is confined at the boundary. We find that the edge states merge into the energy band of the bulk states through bifurcation. The edge-state width is computed for various SOCs and sublattice potentials. We discuss the significant effects variation in the edge-state width has on experimentally measured data.

II. MODEL AND METHOD

We start with the Hamiltonian from the KM model[3] with the creation (annihilation) operator $c_{i\sigma}$ ($c_{i\sigma}^\dagger$) for an electron with spin σ at site i on the honeycomb lattice, i.e.,

$$H = -t \sum_{\langle i,j\rangle\sigma} c_{i\sigma}^\dagger c_{j\sigma} + \lambda_v \sum_{i\sigma} \mu_i c_{i\sigma}^\dagger c_{i\sigma} + i\lambda_{\mathrm{SO}} \sum_{\langle\langle i,j\rangle\rangle\alpha,\beta} \nu_{ij} \sigma_{\alpha\beta}^z c_{i\alpha}^\dagger c_{j\beta}. \quad (1)$$

The first term of this equation describes the hopping of electrons between nearest-neighbor sites $\langle i,j\rangle$ with a hopping

integral t. The staggered sublattice potential of strength λ_v is included in the second term, with $\mu_i = \pm 1$ on each sublattice. The third term is a spin-dependent hopping between next-nearest neighbors $\langle\langle i,j\rangle\rangle$ due to the SOC. $\lambda_{\rm SO}$ is SOC, and σ^z is the z component of the Pauli matrix; $\nu_{ij} = \pm 1$ is determined from $\nu_{ij} = \frac{2}{\sqrt{3}a^2}(\boldsymbol{d}_1 \times \boldsymbol{d}_2)_z$, where $\boldsymbol{d}_1$ and $\boldsymbol{d}_2$ are the unit vectors connecting the sites j and i. Henceforth, we set $a = 1$ for simplicity. The Hamiltonian in Eq. (1) gives the following energy spectrum:

$$E_\sigma(\boldsymbol{k}) = \pm\sqrt{\varepsilon_0(\boldsymbol{k}) + \{2\sigma\lambda_{\rm SO}\varepsilon_1(\boldsymbol{k}) + \lambda_v\}^2}, \tag{2}$$

where $\varepsilon_0(\boldsymbol{k}) = 3 + 2\cos k_x + 4\cos\frac{k_x}{2}\cos\frac{\sqrt{3}}{2}k_y$ and $\varepsilon_1(\boldsymbol{k}) = \sin k_x - 2\sin\frac{k_x}{2}\cos\frac{\sqrt{3}}{2}k_y$, with $\sigma = \pm 1$ depending on the electron spin. It is known that the system has finite gaps of $2|3\sqrt{3}\lambda_{\rm SO} \pm \lambda_v|$ at the two Dirac points $\mathbf{K}$ and $\mathbf{K}'$, indicating that the system is in an insulating state.

One prominent characteristic of the topologically nontrivial phase is that a metallic state emerges at the boundary. To investigate the edge states, we assume a zigzag boundary along the x direction while the system is semi-infinite in the y direction, as shown in Fig. 1. The method that we use in this work is similar to what was employed in the study of the edge state in the integer quantum Hall system on a square lattice.[30,31] By constructing the Harper equation[32,33] with the assumption that the state is localized exponentially at the edge we can write the edge-state wave function in the following form:[13,24]

$$\Psi_{k\sigma,y} = (e^{ik/2}\Lambda)^j \Psi_{k\sigma,y=0}, \tag{3}$$

where $\Psi_{k\sigma,y}$ is a two-component vector whose elements represent the wave functions of spin, σ, for the two bases of the unit cell. Here, k is the momentum in the x direction and j is the site index in the y direction, defined by $y \equiv j(\sqrt{3}a/2)$. Here, Λ is a complex number, the magnitude of which should be less than unity for states localized at the bottom boundary so as to make the wave function decay rapidly as y increases. The effective Hamiltonian for the edge state in Eq. (3) is then given by

$$\hat{H}_{\rm edge} = \begin{bmatrix} -4\lambda_{\rm SO}\sin\frac{k}{2}\left\{\cos\frac{k}{2} - \frac{\Lambda+\Lambda^{-1}}{2}\right\} + \lambda_v & -te^{-ik/2}\left(2\cos\frac{k}{2} + \Lambda^{-1}\right) \\ -te^{ik/2}\left(2\cos\frac{k}{2} + \Lambda\right) & 4\lambda_{\rm SO}\sin\frac{k}{2}\left\{\cos\frac{k}{2} - \frac{\Lambda+\Lambda^{-1}}{2}\right\} - \lambda_v \end{bmatrix} \tag{4}$$

for spin-up electrons. The Hamiltonian for spin-down electrons can be obtained by substituting $-\lambda_{\rm SO}$ for $\lambda_{\rm SO}$.

The following equation should be satisfied for energy E:

$$|\hat{H}_{\rm edge}(\Lambda) - E| = 0. \tag{5}$$

It turns out that this eigenvalue equation is a quadratic function of $\Lambda + \Lambda^{-1}$, yielding four solutions for Λ, i.e., Λ_1, Λ_1^{-1}, Λ_2, and Λ_2^{-1}, with given k and E. (We give this in detailed form together with a derivation in the Appendix.) We can assume that $|\Lambda_2| \leqslant |\Lambda_1| \leqslant 1$ without the loss of generality. Only the two values Λ_1 and Λ_2 are relevant for the description of states localized at the edge of interest. It is clear that the other two—Λ_1^{-1} and Λ_2^{-1}—correspond to edge states at the upper boundary, if any. The wave function may be written as

$$\Psi_{k,y} = C_1(e^{ik/2}\Lambda_1)^j\Phi_{k1} + C_2(e^{-ik/2}\Lambda_2)^j\Phi_{k2}, \tag{6}$$

where Φ_{ki} is the corresponding eigenvector of the solution Λ_i and the energy E in Eq. (5). The wave function vanishes at the boundary of the sample ($j = 0$), which implies that the two eigenvectors are linearly dependent. The condition for the linear dependence of eigenvectors results in the following additional relation (please refer to the Appendix for further details):

$$E + \lambda_v + 4\lambda_{\rm SO}\sin\frac{k}{2}\left(\frac{\Lambda_1+\Lambda_2}{2} + (\Lambda_1\Lambda_2 - 2)\cos\frac{k}{2}\right) = 0. \tag{7}$$

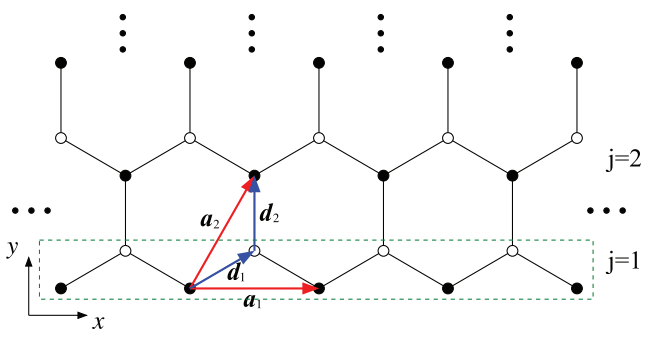

FIG. 1. (Color online) Schematic diagram for the semi-infinite honeycomb lattice with the boundary at the bottom. The lattice is described by the two primitive vectors, $\boldsymbol{a}_1 = a(1,0)$ and $\boldsymbol{a}_2 = \frac{a}{2}(1,\sqrt{3})$ with two bases (0,0) and $\frac{a}{2}(1,1/\sqrt{3})$ in a unit cell.

III. RESULTS

Simple numerical solutions of the coupled Eqs. (5) and (7) produce the energy dispersions of the edge state as well as the corresponding wave functions. In Fig. 2, we show the edge-state energy dispersion for spin-up electrons with various λ_v. The TRS in the system guarantees that the dispersions for the opposite spin are obtained by the inversion of k around $k = \pi$ (not shown in the figure). The resulting dispersion relations clearly demonstrate that a metallic edge state exists inside the finite band gap and that the dispersion relation gradually merges into the bulk states as the crystal momentum

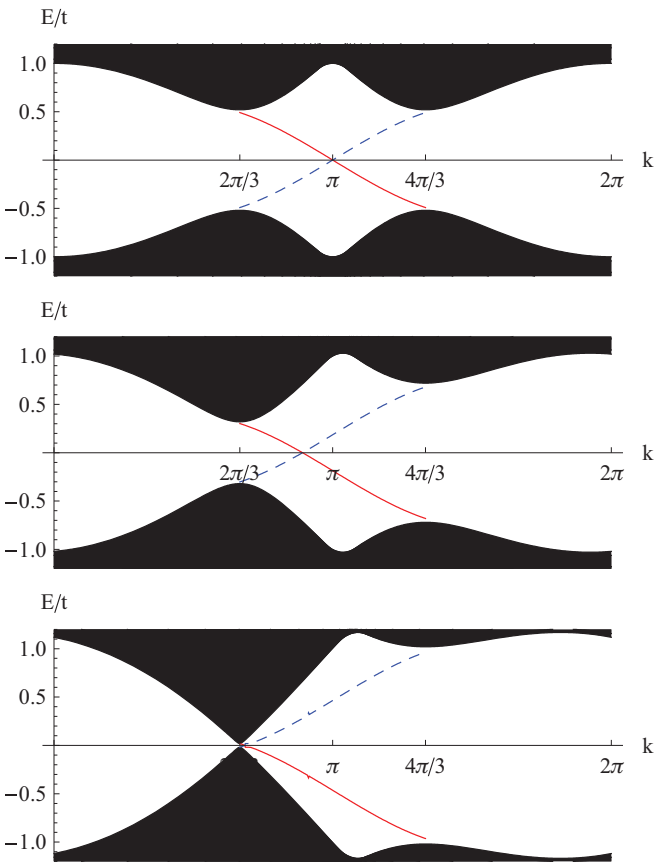

FIG. 2. (Color online) Edge-state energy dispersions for spin-up electrons with $\lambda_{SO}/t = 0.1$ and with $\lambda_v/t = 0.0$ (top), $\lambda_v/t = 0.2$ (middle), and $\lambda_v/t = 0.49$ (bottom). The edge-state dispersion relations at the lower boundary are shown by the (red) solid lines. Those at the upper boundary are shown by the (blue) dotted lines for completeness. The shaded areas represent the bulk energy spectra.

approaches $k = \frac{2\pi}{3}$ or $\frac{4\pi}{3}$. Even when the presence of λ_v induces a difference between the gaps at the two Dirac points and the dispersion relation becomes asymmetric around $k = \pi$, the metallic edge states are preserved. Finally, one of the gaps closes when λ_v reaches the critical value of $3\sqrt{3}\lambda_{SO}$, which makes the whole system metallic. A further increase in λ_v above the critical value opens a gap in the bulk. In this case, however, the bulk is a normal insulator, which is accompanied by a gap at the edge state as well. All the features of the edge-state dispersion relations are fully consistent with the edge-state characteristics revealed by full numerical diagonalization of the KM model with a strip geometry of finite width.[3,29]

Our approach also allows the calculation of the wave functions of the edge states, which is useful for studying the edge-state confinement to the boundary. As the system considered is semi-infinite in the transverse direction, the result is free of size effects due to the finite width of the system. We define an edge-state width ξ_i for each decaying state due to Λ_i in Eq. (3) as

$$\xi_i(k) \equiv \frac{\sqrt{3}}{2}[\ln|1/\Lambda_i(k)|]^{-1}, \tag{8}$$

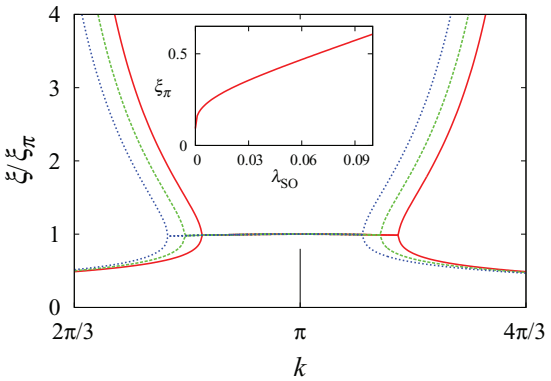

FIG. 3. (Color online) Edge-state width ξ as a function of momentum k for $\lambda_{SO}/t = 0.1$. The data for $\lambda_v/t = 0$, 0.2, and 0.4 are shown by the (red) solid, (green) dashed, and (blue) dot-dashed lines, respectively. Inset: Edge-state width ξ_π for $k = \pi$ as a function of λ_{SO}.

indicating a decay of the form $\sim e^{-y/\xi_i(k)}$. For $k = \pi$, we can solve Eqs. (5) and (7) analytically, yielding

$$\xi_\pi = \frac{\sqrt{3}}{2}\left[\ln\left\{\sqrt{1+\left(\frac{t}{4\lambda_{SO}}\right)^2}+\frac{t}{4\lambda_{SO}}\right\}\right]^{-1}, \tag{9}$$

as described in the Appendix. It is worth noting that, for $k = \pi$ and $|\lambda_v| < \sqrt{t^2 + 16\lambda_{SO}^2}$, the staggered lattice potential λ_v changes only the phase factor of Λ without any effect on ξ_π. (The effect of λ_v on ξ appears for $k \neq \pi$ or larger λ_v, which will be discussed later.) The inset of Fig. 3 shows the behavior of ξ_π as a function of λ_{SO}. The decrease in λ_{SO} makes the wave function narrower. Finally, the edge state is maximally confined at the boundary for $\lambda_{SO} = 0$, which corresponds to the well-known flat-band edge state of the graphene nanoribbon with a zigzag edge.[34] Our results show that ξ vanishes logarithmically $\sim 1/\ln(\lambda_{SO}/t)$ as λ_{SO} approaches zero.

The edge-state widths $\xi_1(k)$ and $\xi_2(k)$ are shown in Fig. 3 for several values of λ_v. In the finite region around $k = \pi$, we find that $\xi_1 = \xi_2$ and that the value is rather insensitive to the variation in k. Above a certain crystal momentum, ξ_1 is no longer identical to ξ_2, and it increases rapidly as k increases with the monotonic decrease of ξ_2. Such behavior of the edge-state width is reminiscent of a bifurcation. Careful examination of Eq. (5) gives us some insight into the origin of the bifurcation: A quadratic equation of $\Lambda + \Lambda^{-1}$ with real coefficients gives two complex roots or two real roots. In the former case, the two complex roots are complex conjugates of each other and ensure that $\Lambda_1 = \Lambda_2^*$, which explains $\xi_1 = \xi_2$ around $k = \pi$. However, this constraint is not imposed for the latter case and $\xi_1 > \xi_2$. Accordingly, the bifurcation occurs only when Eq. (5) has one real double root. It is also noteworthy that ξ_1 diverges at the two Dirac points, where the edge state merges to the energy band of the bulk state. We can verify that, at $k = \pi \pm \pi/3$, the coupled Eqs. (5) and (7) are satisfied by the energy $E = \mp 3\sqrt{3}\lambda_{SO} - \lambda_v$ and $\Lambda_1 = \pm 1$, which guarantees the divergence of ξ_1 and the merging of the edge state to the energy band of extended states at the two Dirac points.

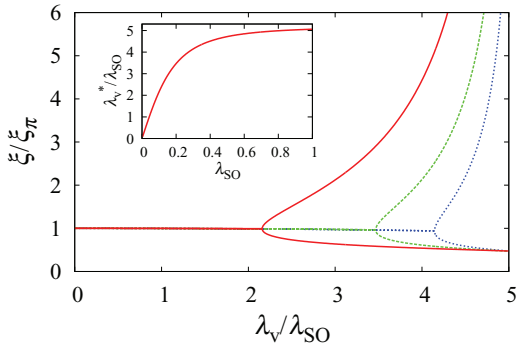

FIG. 4. (Color online) Edge-state width ξ at $E = 0$ as a function of the ratio of the sublattice potential λ_v to SOC λ_{SO}. The data for $\lambda_{SO}/t = 0.1$, 0.2, and 0.3 are denoted by (red) solid, (green) dashed, and (blue) dot-dashed lines, respectively. Inset: Location of the bifurcation value λ_v^* in units of λ_{SO} as a function of λ_{SO}.

The edge-state width has great significance for experiments on samples of a finite width. When ξ is comparable to the sample width, the overlap of the edge states on the opposite boundaries becomes significant, and a finite gap develops in the edge-state dispersion relations. Such effects have been investigated experimentally by varying the film thickness.[22,23]

Experimentally, it is more convenient to tune the edge-state width by applying an external electric field in a sample of fixed width. Silicene, which was recently synthesized,[35–37] provides one interesting possibility. The buckling of two sublattices in silicene enables one to control the sublattice potential λ_v by applying an external electric field.[38] We can also find an interesting realization proposed in an optical lattice[39] where the parameters can be controlled directly. The variation in the edge-state width by changing λ_v, shown in Fig. 4, exhibits a remarkable dependence, particularly around a bifurcation point. Such a dependence is expected to give rise to observable effects on the edge-state gap in narrow samples by the application of an external electric field. It is also interesting that the point λ_v^*, where $\xi(\lambda_v)$ bifurcates, is enhanced by the increase in SOC, which implies that strong SOC pins down the width ξ and suppresses the formation of an edge-state gap up to a higher bifurcation point λ_v^*.

An alternative way to tune the edge-state width in experiments is to control the chemical potential using a gate voltage.[21] In such experiments, the dependence of ξ on the chemical potential shown in Fig. 5 is useful. We have assumed that the band structures do not change significantly in response to variation in the chemical potential. In the absence of the staggered sublattice potential, ξ is not significantly changed by small variations in the chemical potential around the half-filling case ($\mu = 0$). However, when the change in the chemical potential exceeds a bifurcation point, ξ increases rapidly, and gap formation is allowed, with a proper momentum-transferring perturbation. A small increase in λ_v shifts the bifurcation points for both boundaries closer to the Fermi level of a half-filled system, which makes it easier to delocalize the edge states by applying a gate voltage. For large λ_v, the edge states at both boundaries become wider even in the half-filled case. It is interesting that the change in the chemical potential results in an increase in the width of one edge state, while that of the other one is suppressed.

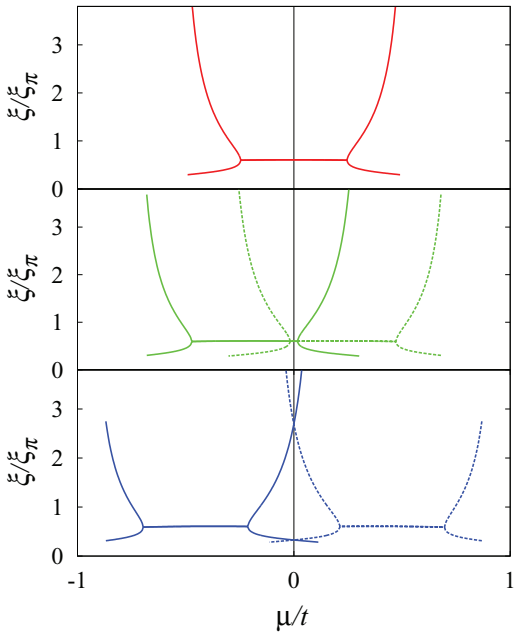

FIG. 5. (Color online) Width of the edge-state for spin-up electrons as a function of the chemical potential μ for $\lambda_v/t = 0$ (top), $\lambda_v/t = 0.2$ (middle), and $\lambda_v/t = 0.4$ (bottom). The solid line corresponds to the edge states at the lower boundary, and the dotted line corresponds to those at the upper boundary.

IV. SUMMARY

We have derived analytical relations for the energies and the width of edge states in the KM model with a zigzag edge. Through the analysis of the width of the edge states, we have shown that a bifurcation of the edge-state width is significant in determining the properties of the edge states. We have also shown that the effects of such a bifurcation can be uncovered by varying experimentally controllable parameters, such as the sublattice potential or the chemical potential.

ACKNOWLEDGMENTS

This work was supported by the National Research Foundation of Korea grant funded by the Korean government under Grants No. 2011-0018306 (H.D.), No. 2008-0061893 (G.S.J.), and No. 2013R1A1A2007959 (G.S.J.).

APPENDIX: DETAILED ANALYSIS OF COUPLED EQUATIONS FOR EDGE STATES

We start with the eigenvalue equation in Eq. (5) for an energy E, which can be written as

$$E^2 - \left[4\lambda_{SO}\sin\frac{k}{2}\left(\cos\frac{k}{2} - X\right) - \lambda_v\right]^2 - t^2\left(4\cos^2\frac{k}{2} + 4X\cos\frac{k}{2} + 1\right) = 0 \qquad \text{(A1)}$$

with

$$X \equiv \tfrac{1}{2}(\Lambda + \Lambda^{-1}). \tag{A2}$$

It is convenient to introduce dimensionless parameters λ_v', t', and $\mathcal{E}$ defined by

$$\lambda_v' \equiv \frac{\lambda_v}{4\lambda_{\mathrm{SO}} \sin\frac{k}{2}}, \tag{A3}$$

$$t' \equiv \frac{t}{4\lambda_{\mathrm{SO}} \sin\frac{k}{2}}, \tag{A4}$$

$$\mathcal{E} \equiv \frac{E}{4\lambda_{\mathrm{SO}} \sin\frac{k}{2}}. \tag{A5}$$

We can then rewrite the eigenvalue equation as a quadratic equation in X:

$$X^2 - 2\left[(1-2t'^2)\cos\frac{k}{2} - \lambda_v'\right]X - \mathcal{E}^2 + t'^2\left(4\cos^2\frac{k}{2} + 1\right) + \left(\lambda_v' - \cos\frac{k}{2}\right)^2 = 0. \tag{A6}$$

The above equation yields two solutions:

$$X_\pm = u \pm \sqrt{v} \tag{A7}$$

with

$$u = (1-2t'^2)\cos\frac{k}{2} - \lambda_v', \tag{A8}$$

$$v = \mathcal{E}^2 - t'^2\left[4(2-t'^2)\cos^2\frac{k}{2} - 4\lambda_v'\cos\frac{k}{2} + 1\right]. \tag{A9}$$

Combined with the definition of X in Eq. (A2), these give four values of Λ:

$$\Lambda_\pm^{(1)} = X_\pm + \sqrt{X_\pm^2 - 1}, \tag{A10}$$

$$\Lambda_\pm^{(2)} = X_\pm - \sqrt{X_\pm^2 - 1} = (\Lambda_\pm^{(1)})^{-1}. \tag{A11}$$

In general, two have magnitudes smaller than 1, and the magnitudes of their inverses are larger than 1. We take Λ_1 and Λ_2 such that $|\Lambda_1| \leqslant |\Lambda_2| \leqslant 1$. The other two are given by Λ_1^{-1} and Λ_2^{-1}. As stated in the main text, we retain only Λ_1 and Λ_2, which correspond to the states bound to the lower edge.

In this way, we can obtain the edge-state wave function for an energy E and a momentum k. Nevertheless, Eq. (A6) alone cannot determine the dispersion relation $E(k)$ of the edge states. To achieve this, we need a second equation, which we will derive from the boundary conditions at the edge.

The edge-state wave function at the lower boundary can be expressed as a linear combination of the two eigenvectors Φ_{k1} and Φ_{k2}, which correspond to Λ_1 and Λ_2, respectively, as shown in Eq. (6). The boundary condition at the lower boundary ($y = 0$) is

$$\Psi_{k,y=0} = 0 = C_1\Phi_{k1} + C_2\Phi_{k2}. \tag{A12}$$

For an edge state with energy E and crystal momentum k to exist, at least one of the coefficients C_1 and C_2 should not vanish. By using the explicit form of the eigenvectors

$$\Phi_{kv} = \begin{bmatrix} \cos\frac{k}{2} - X_v - \lambda_v' - \mathcal{E} \\ t'e^{-ik/2}\left(2\cos\frac{k}{2} + \Lambda_v^{-1}\right) \end{bmatrix} \tag{A13}$$

for $v = 1$ and 2, we can reduce the condition for the existence of the edge state to the form

$$\begin{vmatrix} \cos\frac{k}{2} - X_1 - \lambda_v' - \mathcal{E} & \cos\frac{k}{2} - X_2 - \lambda_v' - \mathcal{E} \\ t'e^{-ik/2}\left(2\cos\frac{k}{2} + \Lambda_1^{-1}\right) & t'e^{-ik/2}\left(2\cos\frac{k}{2} + \Lambda_2^{-1}\right) \end{vmatrix} = 0. \tag{A14}$$

By expanding the above determinant, we obtain the equation

$$\mathcal{E} + \lambda_v' + \frac{\Lambda_1 + \Lambda_2}{2} + (\Lambda_1\Lambda_2 - 2)\cos\frac{k}{2} = 0, \tag{A15}$$

which reduces to Eq. (7) in terms of the original parameters.

For the point $k = \pi$, we can solve the coupled Eqs. (A6) and (A15) analytically. At this point, the equations can be simplified as

$$X_v^2 + 2\lambda_v' X_v - \mathcal{E}^2 + t'^2 + \lambda_v'^2 = 0 \quad (v = 1,2), \tag{A16}$$

$$\mathcal{E} + \lambda_v' + \frac{\Lambda_1 + \Lambda_2}{2} = 0. \tag{A17}$$

We assume that Λ_1 and Λ_2 are complex numbers, which guarantees that Λ_1 and Λ_2 are complex conjugates of each other, as the quartic equation in Eq. (A16) has only real coefficients. They can then be written in terms of the magnitude ρ and the phase θ:

$$\Lambda_1 = \rho e^{i\theta}, \Lambda_2 = \rho e^{-i\theta}. \tag{A18}$$

By substituting

$$X_1 = \frac{1}{2}\left(\rho e^{i\theta} + \frac{1}{\rho}e^{-i\theta}\right) \tag{A19}$$

in Eq. (A16), we obtain

$$\left[\left(\rho + \frac{1}{\rho}\right)\cos\theta + i\left(\rho - \frac{1}{\rho}\right)\sin\theta\right] \times \left[\frac{1}{2}\left(\rho + \frac{1}{\rho}\right)\cos\theta + \lambda_v'\right] - \frac{1}{4}\left(\rho - \frac{1}{\rho}\right)^2 + t'^2 - \mathcal{E}^2 + \lambda_v'^2 - \cos^2\theta = 0. \tag{A20}$$

The boundary condition in Eq. (A17) now reads

$$\mathcal{E} + \lambda_v' + \rho\cos\theta = 0. \tag{A21}$$

Combining the equations in the imaginary part of Eqs. (A20) and (A21), we can express $\mathcal{E}$ and λ_v' in terms of ρ and θ, i.e.,

$$\lambda_v' = -\frac{1}{2}\left(\rho + \frac{1}{\rho}\right)\cos\theta, \tag{A22}$$

$$\mathcal{E} = -\frac{1}{2}\left(\rho - \frac{1}{\rho}\right)\cos\theta, \tag{A23}$$

resulting in the relation

$$\mathcal{E}^2 + \cos^2\theta = \lambda_v'^2. \tag{A24}$$

The real part of Eq. (A20) is then given simply by

$$t'^2 - \frac{1}{4}\left(\rho - \frac{1}{\rho}\right)^2 = 0, \tag{A25}$$

yielding a solution with $0 < \rho \leqslant 1$:

$$\rho = \sqrt{t'^2 + 1} - |t'|. \tag{A26}$$

This gives the edge-state width at $k = \pi$:

$$\xi_\pi = \frac{\sqrt{3}}{2}[\ln\{\sqrt{1 + t'^2} + |t'|\}]^{-1}, \tag{A27}$$

which is given in Eq. (9) in terms of the original parameters. We can also calculate the phase and the energy:

$$\cos\theta = -\frac{\lambda'_v}{\sqrt{t'^2 + 1}}, \tag{A28}$$

$$\mathcal{E} = -\lambda'_v \frac{|t'|}{\sqrt{t'^2 + 1}}. \tag{A29}$$

It is interesting that λ_v does not affect the edge-state width, but only the phase θ. From Eq. (A28) we find that this solution is valid only when $\lambda'_v \leqslant \sqrt{t'^2 + 1}$.

*clotho72@yonsei.ac.kr
†gsjeon@ewha.ac.kr

[1] M. Z. Hasan and C. L. Kane, Rev. Mod. Phys. **82**, 3045 (2010).
[2] X.-L. Qi and S.-C. Zhang, Rev. Mod. Phys. **83**, 1057 (2011).
[3] C. L. Kane and E. J. Mele, Phys. Rev. Lett. **95**, 226801 (2005).
[4] B. A. Bernevig, T. L. Hughes, and S.-C. Zhang, Science (NY) **314**, 1757 (2006).
[5] F. D. M. Haldane, Phys. Rev. Lett. **61**, 2015 (1988).
[6] S.-C. Zhang and J. Hu, Science **294**, 823 (2001).
[7] S. Murakami, N. Nagaosa, and S.-C. Zhang, Science **301**, 1348 (2003).
[8] J. Sinova, D. Culcer, Q. Niu, N. A. Sinitsyn, T. Jungwirth, and A. H. MacDonald, Phys. Rev. Lett. **92**, 126603 (2004).
[9] L. Fu, C. L. Kane, and E. J. Mele, Phys. Rev. Lett. **98**, 106803 (2007).
[10] J. E. Moore and L. Balents, Phys. Rev. B **75**, 121306 (2007).
[11] R. Roy, Phys. Rev. B **79**, 195322 (2009).
[12] M. König, S. Wiedmann, C. Brüne, A. Roth, H. Buhmann, L. W. Molenkamp, X.-L. Qi, and S.-C. Zhang, Science **318**, 766 (2007).
[13] M. König, H. Buhmann, L. W. Molenkamp, T. Hughes, C.-X. Liu, X.-L. Qi, and S.-C. Zhang, J. Phys. Soc. Jpn. **77**, 031007 (2008).
[14] D. Hsieh, D. Qian, L. Wray, Y. Xia, Y. S. Hor, R. J. Cava, and M. Z. Hasan, Nature (London) **452**, 970 (2008).
[15] Y. Xia, D. Qian, D. Hsieh, L. Wray, A. Pal, H. Lin, A. Bansil, D. Grauer, Y. S. Hor, R. J. Cava, and M. Z. Hasan, Nat. Phys. **5**, 398 (2009).
[16] Y. L. Chen, J. G. Analytis, J.-H. Chu, Z. K. Liu, S.-K. Mo, X. L. Qi, H. J. Zhang, D. H. Lu, X. Dai, Z. Fang, S. C. Zhang, I. R. Fisher, Z. Hussain, and Z.-X. Shen, Science **325**, 178 (2009).
[17] D. Hsieh, Y. Xia, D. Qian, L. Wray, J. H. Dil, F. Meier, J. Osterwalder, L. Patthey, J. G. Checkelsky, N. P. Ong, A. V. Fedorov, H. Lin, A. Bansil, D. Grauer, Y. S. Hor, R. J. Cava, and M. Z. Hasan, Nature (London) **460**, 1101 (2009).
[18] P. Roushan, J. Seo, C. V. Parker, Y. S. Hor, D. Hsieh, D. Qian, A. Richardella, M. Z. Hasan, R. J. Cava, and A. Yazdani, Nature (London) **460**, 1106 (2009).
[19] Z. Alpichshev, J. G. Analytis, J.-H. Chu, I. R. Fisher, Y. L. Chen, Z. X. Shen, A. Fang, and A. Kapitulnik, Phys. Rev. Lett. **104**, 016401 (2010).
[20] J. G. Analytis, R. D. McDonald, S. C. Riggs, J.-H. Chu, G. S. Boebinger, and I. R. Fisher, Nat. Phys. **6**, 960 (2010).
[21] J. Chen, H. J. Qin, F. Yang, J. Liu, T. Guan, F. M. Qu, G. H. Zhang, J. R. Shi, X. C. Xie, C. L. Yang, K. H. Wu, Y. Q. Li, and L. Lu, Phys. Rev. Lett. **105**, 176602 (2010).
[22] Y. Zhang, K. He, C.-Z. Chang, C.-L. Song, L.-L. Wang, X. Chen, J.-F. Jia, Z. Fang, X. Dai, W.-Y. Shan, S.-Q. Shen, Q. Niu, X.-L. Qi, S.-C. Zhang, X.-C. Ma, and Q.-K. Xue, Nat. Phys. **6**, 584 (2010).
[23] G. Wang, X. Zhu, J. Wen, X. Chen, K. He, L. Wang, X. Ma, Y. Liu, X. Dai, Z. Fang, J. f. Jia, and Q. Xue, Nano Research **3**, 874 (2010).
[24] Z. Wang, N. Hao, and P. Zhang, Phys. Rev. B **80**, 115420 (2009).
[25] C. Wu, B. A. Bernevig, and S.-C. Zhang, Phys. Rev. Lett. **96**, 106401 (2006).
[26] M. Hohenadler, T. C. Lang, and F. F. Assaad, Phys. Rev. Lett. **106**, 100403 (2011).
[27] D. Zheng, G.-M. Zhang, and C. Wu, Phys. Rev. B **84**, 205121 (2011).
[28] Y. Yamaji and M. Imada, Phys. Rev. B **83**, 205122 (2011).
[29] C. L. Kane and E. J. Mele, Phys. Rev. Lett. **95**, 146802 (2005).
[30] Y. Hatsugai, Phys. Rev. B **48**, 11851 (1993).
[31] Y. Hatsugai, Phys. Rev. Lett. **71**, 3697 (1993).
[32] P. G. Harper, Proc. Phys. Soc. London A **68**, 874 (1955).
[33] D. R. Hofstadter, Phys. Rev. B **14**, 2239 (1976).
[34] M. Fujita, K. Wakabayashi, K. Nakada, and K. Kusakabe, J. Phys. Soc. Jpn. **65**, 1920 (1996).
[35] B. Lalmi, H. Oughaddou, H. Enriquez, A. Kara, S. Vizzini, B. Ealet, and B. Aufray, Appl. Phys. Lett. **97**, 223109 (2010).
[36] P. Vogt, P. De Padova, C. Quaresima, J. Avila, E. Frantzeskakis, M. C. Asensio, A. Resta, B. Ealet, and G. Le Lay, Phys. Rev. Lett. **108**, 155501 (2012).
[37] C.-L. Lin, R. Arafune, K. Kawahara, N. Tsukahara, E. Minamitani, Y. Kim, N. Takagi, and M. Kawai, Appl. Phys. Express **5**, 045802 (2012).
[38] M. Ezawa, Phys. Rev. Lett. **109**, 055502 (2012).
[39] N. Goldman, I. Satija, P. Nikolic, A. Bermudez, M. A. Martin-Delgado, M. Lewenstein, and I. B. Spielman, Phys. Rev. Lett. **105**, 255302 (2010).